

Simulation of Variable Magnetic Field Effect on Natural Convection Heat Transfer of Fe₃O₄/Graphite Slurry based on Experimental Properties of Slurries

I. Pishkar¹, B. Ghasemi^{2†}, A. Raisi², S. M. Aminossadati³

¹ *Department of Mechanics, Payameh Noor University, PO BOX 19395-3697 Tehran, Iran*

² *Engineering Faculty, Shahrekord University, Shahrekord, PO Box 115, Iran*

³ *School of Mechanical Engineering, The University of Queensland, QLD 4072, Australia*

†Corresponding Author Email: ghasemi@eng.sku.ac.ir

(Received January 28, 2021; accepted July 17, 2021)

ABSTRACT

Natural convective heat transfer of Fe₃O₄/graphite slurry in a square cavity is numerically examined. The slurry is assumed to be a non-Newtonian ferrofluid under a variable external magnetic field. The left and right walls of the cavity are assumed to be at a relatively low temperature (T_c), while the horizontal walls are thermally insulated. A heat source with a variable temperature distribution is located at the bottom of the enclosure. The non-Newtonian behavior of the graphite slurry (a mixture of ethylene glycol and graphite powder) has been modelled using experimental results. The control volume method and the SIMPLE algorithm were used to discretize and solve the governing equations considering the Ferro-hydrodynamics (FHD), the Magneto-hydrodynamics (MHD) and the non-Newtonian fluid behavior. The heat transfer and fluid flow properties are determined for different locations of the magnetic field source, and different values of the magnetic number (Kelvin force), and the Hartmann number (Lorentz force). The results show that when the magnetic field source is located below the enclosure and near the heat source, the vortices are strengthened resulting in an increased heat transfer. The heat transfer rate is affected by FHD and MHD. When the magnetic field source is located at the corner points, the heat transfer rate is not significantly affected by the magnetic and Hartmann numbers. However, once the magnetic field source is located near the central point of the lower wall of the enclosure, the heat transfer rate is influenced by the increase of the magnetic number.

Keywords: Ferrofluid; non-Newtonian; Magnetic field; Ferrohydrodynamics (FHD); Magneto-hydrodynamics (MHD).

NOMENCLATURE

\bar{a}, \bar{b}	location of magnetic source	h	convection heat transfer coefficient
a, b	dimensionless location of magnetic source, $a = \bar{a}/L, b = \bar{b}/L$	k	thermal conductivity
A	surface of enclosure	L	enclosure length
B	magnetic induction, $B = \mu_0(H + M)$	$L a_f^*$	extended Hartman number, $L^n \mu_0 H_0 \sqrt{\sigma_f / (\alpha_f^{n-1} \kappa_f)}$
B_x, B_y	magnetic induction components, $B = B_x i + B_y j$	\bar{H}_x, \bar{H}_y	components of the magnetic field intensity ($\bar{H} = \bar{H}_x i + \bar{H}_y j$)
C_p	specific heat	\bar{H}	magnitude of the magnetic field strength
d	perpendicular spacing of the sides of the enclosure	H_x, H_y	dimensionless components of the magnetic field intensity
Ec_f^*	extended Eckert number, $\kappa_f \alpha_f^n / ([\rho C_p]_f [T_h - T_c] L^{2n})$	J	electric current density, $\nabla \times H = \sigma(V \times B)$
g	gravitational acceleration	k	constant parameter
Mn_f^*	extended magnetic number arising from FHD	γ	magnetic field strength at the source

pseudoplastic fluids for the same fully-developed Prandtl numbers. Kefayati (2014) examined the heat transfer from a non-Newtonian molten polymer in a square cavity with sinusoidal wall boundary condition using Finite Difference Lattice Boltzmann Method (FDLBM). Their results showed that the FDLBM is a suitable approach for solving this problem. They showed that heat transfer is generally reduced by increasing the Power-law index. Zhang *et al.* (2015) used the boundary layer theory, and examined the heat transfer and friction of non-Newtonian power-law fluids in the boundary layer. They argued that the velocity profile, power-law index and Prandtl number influenced the distribution of the thermal boundary layer. Moraga *et al.* (2016) used streamlines and isotherms at different Rayleigh numbers to demonstrate the three-dimensional natural convective heat transfer of non-Newtonian power-law fluid in a cavity enclosed by an enclosure. One of the issues that is currently being discussed in the heat transfer processes is the need for a significant increase in heat flux and the reduction in the size of heat transfer equipment. In this regard, an important factor is the effect of thermal properties of the fluids on heat transfer and the application of the magnetic field. Fluids with suspended solid metal particles have higher thermal properties than conventional fluids. The introduction of magnetic field can also affect the process. In this study, Fe_3O_4 nanoparticles that are sensitive to the magnetic field are used. The study of nanofluids heat transfer under a constant magnetic field has been reported in the literature (Aminossadati *et al.* 2014; Aminossadati *et al.* 2011; Ghasemi *et al.* 2011; Kasaeipoor *et al.* 2015; Mahmoudi *et al.* 2013; Rahman *et al.* 2013; Rashad 2017). In all of these investigations, the magnetic field causes a change in the heat transfer from the enclosure in addition to the buoyancy forces and inertia. The constant magnetic field creates a source term in the equations and a magnetohydrodynamic effect on the flow and heat transfer.

In practical situations, the magnetic field generated by an electric current (Current conductor wire) is not constant. That's why most studies have examined the heat transfer in a variable magnetic field. (Ashouri *et al.* (2010) studied natural convection heat transfer of a ferrofluid flow under a variable magnetic field in a square cavity. A permanent magnet with a rectangular dimension was located at a certain distance close to the bottom of the enclosure. The effects of buoyancy inductive flow were neglected. The Langevin model was used for modeling of magnetism. The results were depicted as a function of the Nusselt number on the walls. Tzirtzilakis and Xenos (2013) studied the flow of biomagnetic fluid in a cavity. The enclosure was under the influence of local steady magnetic field. A mathematical model was developed to formulate the problem included the ferrohydrodynamics and magnetohydrodynamics laws. The biomagnetic fluid was assumed to be a homogeneous Newtonian fluid under the influence of an electrical current conductor, having a magnetizing property. The results showed that the magnetic field affected the velocity field. The study focused only on the velocity field and the heat

transfer was not considered. Selimefendigil *et al.* (2014) studied the influence of magnetic field and its local position on the fluid flow and heat transfer of a ferrofluid in an enclosure that was partially heated. The forced convective heat transfer of a ferrofluid in an open enclosure with a rotating cylinder was investigated by (Selimefendigil and Öztop (2014). The main of their study was to examine the effects of magnetic field and angular velocity on the heat transfer.

Natural convection heat transfer from a ferrofluid under constant and variable magnetic field was examined by Yarahmadi *et al.* (2015). They observed that the heat transfer increased for a variable magnetic field; whilst, the heat transfer decreased for a constant magnetic field. They argued that for low Reynolds numbers and high solid-volume fractions, the effect of magnetic field was more significant. In addition, the effect of the oscillation frequency on the local heat transfer depends on oscillatory modes. The influence of magnetic field on laminar convection heat transfer for a ferrofluid flow in a spiral stainless tube was studied by Asfer *et al.* (2016). They argued that the variation of heat transfer coefficient was a function of several parameters such as the fluid thermal conductivity, the ferrofluid flow interaction, the ratio of magnetic to inertia force, and the nanoparticle accumulation near the wall.

A review of the literature indicates that most researchers have used non-Newtonian power-law model in their analysis due to the lack of information and experimental results for the stress-strain behavior of non-Newtonian fluid. The present study uses the experimental properties of the fluid to determine the actual stress-strain relationship of matter. The relationship is used in the governing equations of momentum and energy. It is also concluded that the effect of MHD or FHD has been considered and both effects have not been studied for a given non-Newtonian fluid. Experimental results regarding the behavior Fe_3O_4 / graphite under the variable magnetic field are used to study the effect of the position of the magnetic field on the heat transfer and fluid flow in an enclosure. All properties of fluid that vary with the temperature are obtained from industrial and experimental references. The flow and heat transfer equations were numerically solved using a FORTRAN software code.

2. DESCRIPTION OF THE PROBLEM AND GOVERNING EQUATIONS

A schematic diagram of the square is presented in Fig. 1. It is assumed that the enclosure is filled with different lubricants and Fe_3O_4 nanoparticles ($\phi = 0.03$). A mixture of ethylene glycol and graphite powder (graphite slurry) forms the lubricants with non-Newtonian behavior (Dareing and Dayton 1992). A uniform temperature (T_c), is considered for the right and left walls; and the other walls are assumed to be thermally insulated. The heat source partially mounted on the bottom wall of the enclosure is assumed to have a sinusoidal

temperature distribution. Equation (1) presents the oscillatory temperature profile of the heat source.

$$T_h(x) = T_c + (T_{h_{\max}} - T_c) \sin(\pi x / L) \quad (1)$$

$$\Rightarrow \theta_h(X) = \sin(\pi X), 0.25 \leq X \leq 0.75$$

The oscillatory temperature of the heat source is simulated by an electronic component having a pulse input voltage (Ghasemi 2005). The heat source has a length of $W_{so} = w_{so}/L = 0.5$ and is located at $X_{so} = x_{so}/L = 0.5$. A magnetic field source $H(x, y)$ is located in one of the four positions at a distance (d) from the sides of the enclosure, whose position is determined by the coordinates (a, b).

The density variations are simulated by using the Boussinesq approximation and the fluid flow is assumed to be incompressible and laminar. The flow in the cavity is also bidirectional and steady.

The acceleration of gravity is constant and in the negative direction of y ($g = -9.81m/s^2$).

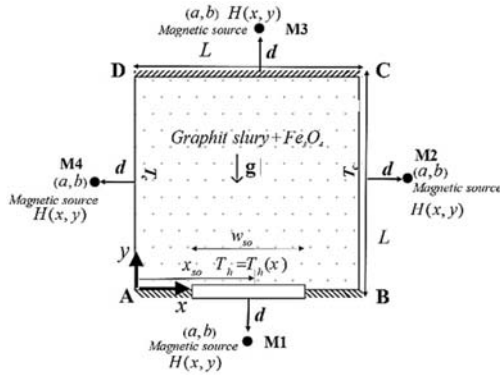


Fig. 1. A schematic diagram of the physical model.

The magnetic nanofluid (ferrofluid) is influenced by the magnetic field. Therefore, two main forces will be applied to nanofluid. First is the magnetic force that depends on the tendency of the particles to coincide with the magnetic field (Kelvin force). Second is the Lorentz force that depends on the motion of the ions (electric charges) in the magnetic field (Rosensweig 2013). Governing equations of the problem include the mass conservation, momentum and their combination, presented in Eqs. (4) to (6) (Tzirtzilakis 2005; Vinogradov *et al.* 2011).

$$\text{Kelvin Force} = \mu_0 (\mathbf{M} \cdot \nabla) \mathbf{H} \quad (2)$$

$$\text{Lorentz Force} = \mathbf{J} \times \mathbf{B} \quad (3)$$

$$\frac{\partial u}{\partial x} + \frac{\partial v}{\partial y} = 0 \quad (4)$$

$$\rho_{ff} \left(u \frac{\partial u}{\partial x} + v \frac{\partial u}{\partial y} \right) = -\frac{\partial p}{\partial x} + \frac{\partial \tau_{xx}}{\partial x} + \frac{\partial \tau_{xy}}{\partial y} \quad (5)$$

$$+ \mu_0 M \frac{\partial \bar{H}}{\partial x} - \sigma_{ff} B_y^2 u + \sigma_{ff} B_x B_y v$$

$$\rho_{ff} \left(u \frac{\partial v}{\partial x} + v \frac{\partial v}{\partial y} \right) = -\frac{\partial p}{\partial y} + \frac{\partial \tau_{xy}}{\partial x} + \frac{\partial \tau_{yy}}{\partial y} \quad (6)$$

$$+ \rho_{ff} g \beta_{ff} (T - T_c) + \mu_0 M \frac{\partial \bar{H}}{\partial y}$$

$$- \sigma_{ff} B_x^2 v + \sigma_{ff} B_x B_y u$$

Since the ferrofluid particles are affected by the magnetic field, this force is very effective in the heat transfer of the fluid, because it increases the fluid motion. Two terms are added to the energy equation for the ferrofluid under the influence of the magnetic field: the term $\mu_0 T (\partial M / \partial T) (DH / DT)$ that expresses the thermal energy per unit volume depends on the magnetocaloric effect. This term deals with the effects of ferrohydrodynamics. The term $\mathbf{J} \cdot \mathbf{J} / \sigma$ is Joule heating that \mathbf{J} is electric current density, $\mathbf{J} = \nabla \times \mathbf{H} = \sigma (\mathbf{V} \times \mathbf{B})$, A/m^2 . This term is related to the effects of magnetohydrodynamics (Rosensweig 2013). Combining these two terms in the energy equation results in:

$$(\rho C_p)_{ff} \left(u \frac{\partial T}{\partial x} + v \frac{\partial T}{\partial y} \right) = \frac{\partial}{\partial x} \left(k_{ff} \frac{\partial T}{\partial x} \right) + \quad (7)$$

$$\frac{\partial}{\partial y} \left(k_{ff} \frac{\partial T}{\partial y} \right) + \sigma_{ff} (u B_y - v B_x)^2$$

$$- \mu_0 T \frac{\partial M}{\partial T} \left(u \frac{\partial \bar{H}}{\partial x} + v \frac{\partial \bar{H}}{\partial y} \right)$$

The graphite slurry is a non-Newtonian fluid. The relationship between the shear stress and the strain rate is given by (Dareing and Dayton 1992):

$$\tau_{ij} = \kappa \dot{\gamma}_{ij}^n = (\kappa \dot{\gamma}_{ij}^{n-1}) \dot{\gamma}_{ij} = 2 \mu_{aij} \dot{\gamma}_{ij} \quad (8)$$

$$\dot{\gamma}_{ij} = \frac{1}{2} \left(\frac{\partial u_i}{\partial x_j} + \frac{\partial u_j}{\partial x_i} \right)$$

Based on the above relations, the apparent viscosity is:

$$\text{Apparent viscosity} \quad (9)$$

$$= \mu_{aij} = \frac{1}{2} \kappa \dot{\gamma}_{ij}^{n-1} = \frac{\kappa}{2} \left(\frac{1}{2} \left[\frac{\partial u_i}{\partial x_j} + \frac{\partial u_j}{\partial x_i} \right] \right)^{n-1}$$

The values of κ and n as a function of temperature are given in Table 1.

Table 1 the values of κ and n as a function of temperature for Graphite slurry (Dareing and Dayton 1992)

$^{\circ}C$ (T)	$\kappa(Pa.s^n)$	n
20	0.0572	0.973
30	0.0448	0.971
40	0.0390	0.969
50	0.0361	0.969

The two-dimensional required stresses are:

$$\begin{aligned} \tau_{xx} &= 2\mu_{axx}\dot{\gamma}_{xx} & \mu_{axx} &= \frac{\kappa}{2} \left(\frac{\partial u}{\partial x} \right)^{n-1} \\ \tau_{xy} &= 2\mu_{axy}\dot{\gamma}_{xy} & \mu_{axy} &= \frac{\kappa}{2} \left(\frac{1}{2} \left[\frac{\partial u}{\partial y} + \frac{\partial v}{\partial x} \right] \right)^{n-1} \\ \tau_{yy} &= 2\mu_{ayy}\dot{\gamma}_{yy} & \mu_{ayy} &= \frac{\kappa}{2} \left(\frac{\partial v}{\partial y} \right)^{n-1} \end{aligned} \quad (10)$$

Equations for the magnetic field are given in references 9 and 10, according to reference (Tzirtzilakis 2005).

$$\begin{aligned} \bar{H}_x &= \frac{\gamma}{2\pi} \frac{1}{(x-\bar{a})^2 + (y-\bar{b})^2} (y-\bar{b}) \\ \bar{H}_y &= -\frac{\gamma}{2\pi} \frac{1}{(x-\bar{a})^2 + (y-\bar{b})^2} (x-\bar{a}) \\ \bar{H} &= \bar{H}_x \mathbf{i} + \bar{H}_y \mathbf{j} \\ \bar{H} &= \sqrt{(\bar{H}_x^2 + \bar{H}_y^2)} = \frac{\gamma}{2\pi} \frac{1}{\sqrt{(x-\bar{a})^2 + (y-\bar{b})^2}} \end{aligned} \quad (11)$$

where \bar{a}, \bar{b} are the magnetic field source coordinates, γ represents the strength of the magnetic field and \bar{H}_y, \bar{H}_x are the intensity components of the magnetic field.

$$\mathbf{M} = k\bar{H}(T'_c - T) \text{ or } M = k'\bar{H}(T'_c - T) \quad (12)$$

In Eq. 12, k' is a constant value and T'_c represents the Curie temperature and both are related to the fluid material. In general, in various materials, the excess of the temperature increases the vibrations of the atoms and the atoms cannot rotate well. As a result, the magnetic property of ferrofluid is destroyed. The temperature that causing it to occur is Curie temperature. The Curie temperature for Fe_3O_4 nanoparticles is $T'_c = 738K$ (Blaney 2007). According to the definition of vectors H and M :

$$\mathbf{B} = \mu_0(\mathbf{H} + \mathbf{M}) \quad (13)$$

B_x, B_y are the components of magnetic induction.

2.1. Properties of Non-Newtonian ferrofluid

Table 2 presents the equations that can be used to calculate the properties of the non-Newtonian ferrofluid as a function of the properties of the graphite slurry (f) and the properties of the Fe_3O_4 nanoparticles (s) (Sheikholeslami and Ganji 2014).

2.1.1. Graphite slurry

The graphite slurry is a mixture of ethylene glycol and graphite particles (mass ratio of 8 to 1) (Dareing and Dayton 1992). The properties of ethylene glycol is determined using the tool box provided by (Anon n.d.) and the properties of graphite particles are determined using the experimental data from POCO graphit-an Entegris company (Anon 2015) as well as the data from the study conducted by Yue *et al.* (2012), Mostofizadeh *et al.* (2011) and Raisi *et al.* (2016). The graphite slurry properties are a function of temperature given by:

Specific heat of graphite slurry:

$$\begin{aligned} (\rho C_p)_f &= 2.599732 \times 10^6 + 5087.77T \\ &- 3.532 \times 10^{10} (T + 273.15)^{-2} \\ &+ 6.225 \times 10^{12} (T + 273.15)^{-3} \end{aligned} \quad (14)$$

Thermal conductivity of graphite slurry:

$$\begin{aligned} k_f &= (0.30427 - 7.6310 \times 10^{-4}T + 6.4806 \times 10^{-8}T^2) \times \\ &\left(\frac{-2.244 \times 10^{-8}T^3 + 1.011 \times 10^{-4}T^2 - 0.1433T + 135.186}{-1.87 \times 10^{-8}T^3 + 8.46 \times 10^{-5}T^2 - 0.1203T + 113.28} \right) \end{aligned} \quad (15)$$

Consistency index of graphite slurry according to Table 1:

$$\kappa_f = \frac{0.4237 + 0.02468T}{-3.96 + T} \quad (16)$$

The Celsius temperature scale is used in these relationships.

2.1.2. Fe_3O_4 nanoparticles

Fe_3O_4 nanoparticles have magnetic properties. Their specific gravity is obtained using the data of the reference (Westrum Jr and Grønbold 1969) and using the curve fitting as follows:

Specific heat of Fe_3O_4 :

$$(\rho C_p)_s = 5200 \times (1.12T + 623.11) \quad (17)$$

The Celsius temperature scale is used in this relationship.

The ferrofluid properties can be determined by combining the properties of the graphite slurry and the properties of Fe_3O_4 nanoparticles according to Table 2.

Table 2 Properties of Graphite Slurry+Fe3O4 Non-Newtonian ferrofluid

Ferrofluid density: $\rho_{ff} = \rho_f(1-\phi) + \rho_s\phi$
Specific heat of the ferrofluid: $(\rho C_p)_{ff} = (\rho C_p)_f(1-\phi) + (\rho C_p)_s\phi$
Ferrofluid Thermal conductivity (Karimi <i>et al.</i> 2015): $k_{ff} = \left(1 + \phi + a\phi \left[\frac{T}{T_{min}}\right]^b\right) k_f$, $a = 119.22, b = 0.06423, T_{min} = 20^\circ C$
Consistency index of ferrofluid (Li <i>et al.</i> 2016): $\kappa_{ff} = (150\phi^2 + 2.5\phi + 1) \kappa_f$
Electrical conductivity of ferrofluid: $\frac{\sigma_{ff}}{\sigma_f} = 1 + \frac{3(\frac{\sigma_s}{\sigma_f} - 1)\phi}{(\frac{\sigma_s}{\sigma_f} + 2) - (\frac{\sigma_s}{\sigma_f} - 1)\phi}$
Thermal expansion coefficient of ferrofluid: $(\rho\beta)_{ff} = (\rho\beta)_f(1-\phi) + (\rho\beta)_s\phi$

Specific heat of ferrofluid:

$$(\rho C_p)_{ff} = \phi \times 5200 \times (1.12T + 623.11) + (1 - \phi) \times \left(2.599732 \times 10^6 + 5087.77T - 3.532 \times 10^{10}(T + 273.15)^{-2} + 6.225 \times 10^{12}(T + 273.15)^{-3} \right) \quad (18)$$

Thermal conductivity of ferrofluid:

$$k_{ff} = \left(1 + \phi + 119.22\phi \left[\frac{T}{20}\right]^{0.06423}\right) \times \left(0.30427 - 7.6310 \times 10^{-4}T + 6.4806 \times 10^{-8}T^2\right) \times \left(\frac{-2.244 \times 10^{-8}T^3 + 1.011 \times 10^{-4}T^2 - 0.1433T + 135.186}{-1.87 \times 10^{-8}T^3 + 8.46 \times 10^{-5}T^2 - 0.1203T + 113.28}\right) \quad (19)$$

Consistency index of ferrofluid:

$$\kappa_{ff} = (150\phi^2 + 2.5\phi + 1) \times \left(\frac{0.4237 + 0.02468T}{-3.96 + T}\right) \quad (20)$$

Thermophysical properties of Graphite slurry and Fe₃O₄ nanoparticles are presented in Table 3:

Table 3 Thermophysical properties of Graphite slurry and Fe₃O₄ nanoparticles

	ρ (kg / m ³)	β $\times 10^5 (K^{-1})$	σ ($\Omega.m$) ⁻¹
Graphite slurry	1180	57	1.278×10^{-4}
Fe ₃ O ₄	5200	1.3	25000

In general, experimental correlations are valid in the temperature range between 20°C and 90°C.

2.2. Dimensionless governing equations

The following non-dimensional parameters are used in the analysis:

$$X = \frac{x}{L}, Y = \frac{y}{L}, U = \frac{uL}{\alpha}, V = \frac{vL}{\alpha}, P = \frac{\bar{p}L^2}{\rho\alpha^2}, \theta = \frac{T - T_c}{\Delta T}, \Delta T = T_{hmax} - T_c, \quad (21)$$

$$H_0 = \bar{H}(a, 0) = \frac{\gamma}{2\pi|b|}$$

The following non-dimensional governing equations are presented:

$$\frac{\partial U}{\partial X} + \frac{\partial V}{\partial Y} = 0 \quad (22)$$

$$U \frac{\partial U}{\partial X} + V \frac{\partial U}{\partial Y} = -\frac{\partial P}{\partial X} + Pr^* \left(\frac{\partial}{\partial X} \left[2\mu'_{axx} \frac{\partial U}{\partial X} \right] + \frac{\partial}{\partial Y} \left[\mu'_{axy} \left\{ \frac{\partial U}{\partial Y} + \frac{\partial V}{\partial X} \right\} \right] \right) + \left(Mn_f^* \cdot Pr_f^* \left[\frac{\rho_f}{\rho_{ff}} \right] \left[\varepsilon_2 - \varepsilon_1 - \theta \right] \right) \times H \frac{\partial H}{\partial X} - (Ha_f^*)^2 \cdot Pr_f^* \left(\frac{\sigma_{ff} / \sigma_f}{\rho_{ff} / \rho_f} \right) \left(H_y^2 U - H_x H_y V \right) \quad (23)$$

$$U \frac{\partial V}{\partial X} + V \frac{\partial V}{\partial Y} = -\frac{\partial P}{\partial Y} + Pr^* \left(\frac{\partial}{\partial X} \left[\mu'_{axy} \left\{ \frac{\partial U}{\partial Y} + \frac{\partial V}{\partial X} \right\} \right] + \frac{\partial}{\partial Y} \left[2\mu'_{yy} \frac{\partial V}{\partial Y} \right] \right) + Mn_f^* \cdot Pr_f^* \left(\frac{\rho_f}{\rho_{ff}} \right) \left(\varepsilon_2 - \varepsilon_1 - \theta \right) H \frac{\partial H}{\partial Y} - (Ha_f^*)^2 \cdot Pr_f^* \left(\frac{\sigma_{ff} / \sigma_f}{\rho_{ff} / \rho_f} \right) \left(H_x^2 V - H_x H_y U \right) + Ra_f^* \cdot Pr_f^* \left(\frac{(\rho\beta)_{ff}}{\rho_{ff} \beta_f} \right) \theta \quad (24)$$

$$\begin{aligned}
 U \frac{\partial \theta}{\partial X} + V \frac{\partial \theta}{\partial Y} &= \frac{\partial}{\partial X} \left(kk \frac{\partial \theta}{\partial X} \right) + \frac{\partial}{\partial Y} \left(kk \frac{\partial \theta}{\partial Y} \right) + \\
 (Ha_f^*)^2 . Ec_f^* &\cdot \left[\frac{\sigma_{ff} / \sigma_f}{(\rho C_p)_{ff} / (\rho C_p)_f} \right] \cdot \{UH_y - VH_x\}^2 \\
 + Mn_f^* . Ec_f^* &\cdot \frac{(\rho C_p)_f}{(\rho C_p)_{ff}} \left\{ U \frac{\partial H}{\partial X} + V \frac{\partial H}{\partial Y} \right\} H(\varepsilon_1 + \theta) \\
 \left[\frac{k_{ff} / k_f}{(\rho C_p)_{ff} / (\rho C_p)_f} \right] &= kk
 \end{aligned} \tag{25}$$

The non-dimensional numbers that are used in the above equations are given in Table 4:

Table 4 Non-dimensional numbers used in Eqs. (21) to (25)

Extended Prandtl number: $Pr_f^* = \frac{\kappa_f}{\rho_f \alpha_f^{2-n} L^{2n-2}}$
Apparent viscosity:
$\mu'_{axy} = 0.5 \left(0.5 \left[\frac{\partial U}{\partial Y} + \frac{\partial V}{\partial X} \right] \right)^{n-1}$
$\mu'_{axx} = 0.5 \left(\frac{\partial U}{\partial X} \right)^{n-1}$ $\mu'_{ayy} = 0.5 \left(\frac{\partial V}{\partial Y} \right)^{n-1}$
Extended Hartman number:
$Ha_f^* = L^n \mu_0 H_0 \sqrt{\sigma_f / (\alpha_f^{n-1} \kappa_f)}$
Temperature number: $\varepsilon_1 = \frac{T_c}{T_{h \max} - T_c}$
Curie temperature number: $\varepsilon_2 = \frac{T_c'}{(T_{h \max} - T_c)}$
Extended Rayleigh number:
$Ra_f^* = \frac{g \beta_f L^{2n+1} (T_{h \max} - T_c) \rho_f}{\kappa_f \alpha_f^n}$
Extended Eckert number:
$Ec_f^* = \frac{\kappa_f \alpha_f^n}{[(\rho C_p)_f] [T_{h \max} - T_c] L^{2n}}$
Extended Magnetic number:
$Mn_f^* = \frac{\mu_0 H_0^2 k' (T_{h \max} - T_c) L^{2n}}{\alpha_f^n \kappa_f}$

2.3 Boundary conditions

The following boundary conditions are used in the analysis:

$$\begin{aligned}
 U = V = 0 & \quad \text{For the enclosure walls} \\
 \theta = 0 & \quad \text{For the left and right walls} \\
 \frac{\partial \theta}{\partial Y} = 0 & \quad \text{For insulation walls} \\
 \theta = \sin(\pi X), & \quad \text{For the heat source} \\
 0.25 \leq X \leq 0.75 &
 \end{aligned}$$

3. NUMERICAL METHOD

A control volume approach using a power law profile approximation is used to discretise the non-dimensional governing equations presented in Eqs. (22)–(25). The power-law model is used to discretize the advection and diffusion terms and the second order central difference scheme is used for other derivatives. The SIMPLE algorithm is used to solve the set of discretised governing equations using the corresponding boundary conditions given in section 3.3. After solving the governing equations for U, V and θ , other useful quantities such as Nusselt number can be determined. (Patankar 1980).

The convergence was determined by:

$$\sum_j \sum_i \sqrt{\left(\frac{\phi^{n+1} - \phi^n}{\phi^{n+1}} \Big|_{i,j} \right)^2} \leq 10^{-7} \tag{26}$$

where n denotes the number of iterations and ϕ is a parameter that can be U, V or θ . Generally, the system is programmed and modeled using FORTRAN software.

The local Nusselt number on the heat source is given by:

$$Nu_{so} = - \frac{k_{ff}}{k_f} \frac{\partial \theta}{\partial Y} \Big|_{Y=0.0}, \quad 0.25 \leq X \leq 0.75 \tag{27}$$

The average Nusselt number is given by:

$$Nu_m = \frac{1}{W_{so}} \int_{X_s - 0.5W_{so}}^{X_s + 0.5W_{so}} Nu_{so}(X) dX \tag{28}$$

The change of Nusselt number is given by:

$$\eta = \frac{Nu_m|_{Mn} - Nu_m|_{Mn=0}}{Nu_m|_{Mn}} \times 100 \tag{29}$$

The average temperature of the ferrofluid is given by:

$$\theta_{avg} = \frac{1}{A' \text{ domain}} \iint \theta(X, Y) dXdY \tag{30}$$

3.1 Grid independency

An appropriate grid is selected so that the results are independent of the number of grid points. For the case, where the magnetic field source is in the

position (M1) with a coordinate of $(a, b) = (0.5, -0.1)$ (refer to Fig. 1), the results for the five different grid sizes are shown in Table 5. According to the results, the grid resolution of 80×80 is selected for further simulations. The last row of the table 5 shows the percentage of the difference between the 120×120 grid and the 80×80 grid.

Table 5 Effect of the number of grid points on average Nusselt number

Number of grid points	Nu_m			
	$Mn_f^* = 10^3$		$Mn_f^* = 10^6$	
	$Ha_{f=5}^*$	$Ha_{f=100}^*$	$Ha_{f=5}^*$	$Ha_{f=100}^*$
40 × 40	11.557	6.531	21.355	11.014
60 × 60	11.623	6.586	18.70	9.309
80 × 80	11.723	6.667	13.967	8.419
100 × 100	11.725	6.669	13.958	8.392
120 × 120	11.726	6.670	13.950	8.390

3.2 Validation

The validation of the numerical model is carried out by comparing the average Nusselt number from [Turan *et al.* \(2011\)](#) and the present study at $Pr=100$, different Rayleigh numbers ($Ra=10^4$ and 10^5) for $n=0.6, n=1.0$ and $n=1.4$. The results are tabulated in Table 6. The results indicate that the present numerical model is in good agreement with [Turan *et al.* \(2011\)](#) with a maximum error below 4%.

The present code is further validated by applying the magnetic field and comparing the results against the study by [Ghasemi *et al.* \(2011\)](#). The results of this comparison in terms of the Nusselt number is shown in Fig. 2. [Ghasemi *et al.* \(2011\)](#) studied the effect of magnetic field on natural convection in a square enclosure filled with nanofluid. In their study, the nanofluid was under a uniform magnetic field in the direction of the x-axis whose geometry is given in Fig. 2. The studied range of the Rayleigh and Hartmann numbers was $10^3 \leq Ra \leq 10^7$ and $0 \leq Ha \leq 60$, respectively. It is observed that there is a very slight difference between the Nusselt numbers.

4. RESULTS

Once the grid study and the code validation is completed, the effects of the magnetic field position, the Kelvin force (magnetic number) and the Lorentz force (Hartmann number) on the heat transfer rate and fluid flow are investigated. Since the fluid is Fe_3O_4 / graphite nanofluid, the constant values are

$Ra_f^* = 10^5, Pr_f^* = 283, Ec_f^* = 10^{-8}, \epsilon_1 = 0.0, \epsilon_2 = 15$. The results are presented in two sections.

Table 6 Comparison of the average Nusselt number obtained from the present study with numerical results obtained by [Turan *et al.* \(2011\)](#).

Ra	Turan <i>et al.</i> (2011)	Present study	Max Difference (%)
10^4 $n=0.6$	5.70903	5.93148	3.89
10^5 $n=0.6$	12.98500	13.29871	
10^4 $n=1.0$	2.40512	2.42125	2.75
10^5 $n=1.0$	4.72576	4.59123	
10^4 $n=1.4$	1.35514	1.32541	2.63
10^5 $n=1.4$	2.28945	2.22142	

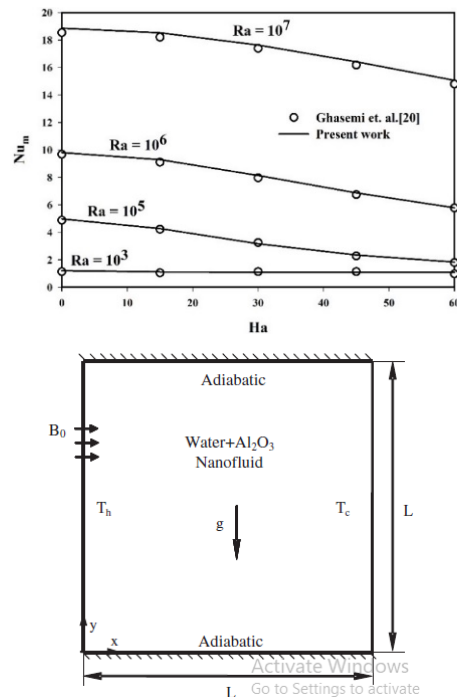


Fig. 2. Schematic of the problem ([Ghasemi *et al.* 2011](#)) (bottom) and the validation: average Nusselt number with Hartmann number $\phi = 0.03$ (top).

- In the first section, the magnetic and Hartmann numbers are assumed to be constant ($Mn_f^* = 10^4$ and $Ha_f^* = 100$), and the effects of the magnetic field position on the heat transfer rate and fluid flow are examined. Furthermore, the optimal position of the magnetic source is studied.
- In the second section, the effects of the Kelvin and Lorentz forces on the heat transfer rate and the fluid flow are examined.

4.1. Effect of the magnetic source position

Considering that the location of the magnetic source is one of the important parameters in the process of heat transfer under the magnetic field, in this section the effect of the magnetic field position on the flow and temperature fields, as well as the heat transfer rate, is investigated.

4.1.1. Displacement of the magnetic field source on the four sides of the enclosure

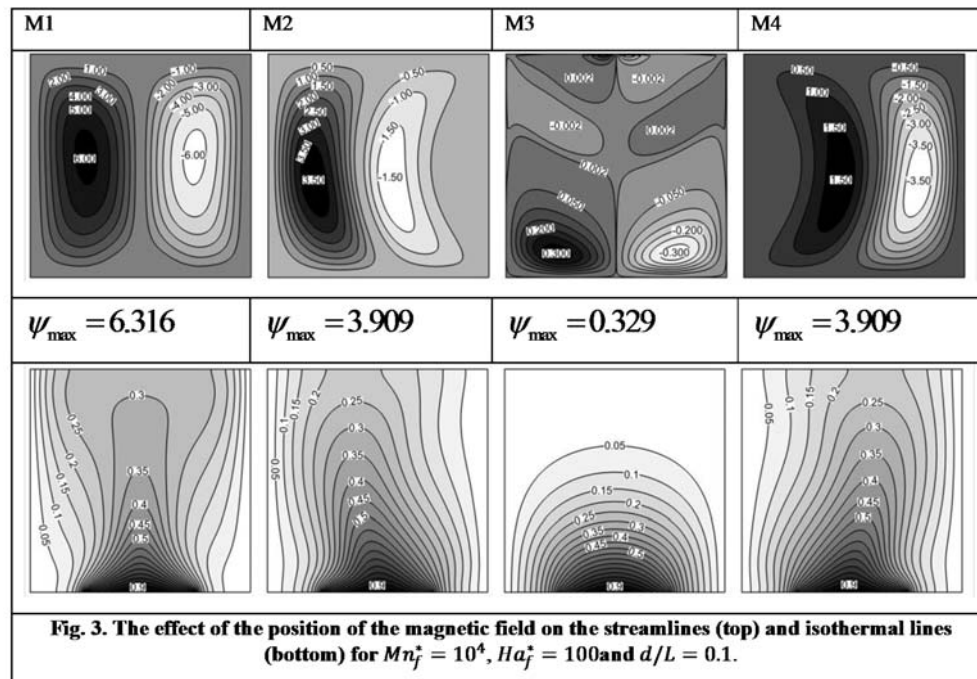
Figure 3 shows the effects of the position of magnetic field source on the streamlines and isothermal lines. The location of the magnetic field is considered to be at four points of M1, M2, M3 and M4, which are at a distance of $d/L = 0.1$, from the center of the bottom wall (AB), right wall (BC), top wall (CD) and left one (DA), respectively (see Fig. 1).

In all cases (except case M3), two counter-rotating vortices are formed inside the enclosure. The formed vortices are symmetrical when the magnetic source is located at points M1 and M3. According to the direction of rotation of the vortices and also direction of the Lorentz and Kelvin forces, the strength of the

vortices has a maximum value when the magnetic source is at point M1 and it has a minimum amount when the magnetic source is at point M3. As the streamlines indicate, the vortices become asymmetric when the magnetic source is placed at the points M2 and M4. In these cases, the vortex which is near the magnetic source decreases and this weakened vortex is shifted to the opposite side. It is also evident that when the source of the magnetic field is at the point M1, two large and strong vortices are formed in the enclosure and the heat transfer is maximal according to Fig. 4. It is also clear from the isotherms that these lines have more dispersion in the enclosure, resulting in more heat transfer.

In the case of a magnetic field located at the point M3, two small and weak vortices are formed in the lower part of the enclosure and the heat transfer has the lowest value (see Fig. 4). Due to the symmetry of the enclosure, when the source of the magnetic field is positioned at the points M2 or M4, the magnetic field weakens the vortex near its side and displaces it towards the vortex of the other side. Isothermal lines are also directed to the opposite side. In general, it can be said that when the source of the magnetic field is close to the source of heat generation, the strength of the vortices and the heat transfer increase due to the direction of the magnetic field and vortices. When it is far from the heat generation source, the strength of the vortices and the heat transfer decrease.

Table 7 also shows the average Nusselt number and its percentage increase for the four positions of the magnetic field source. The maximum percentage increase in average Nusselt number compared to the



absence of a magnetic field corresponds to the point M1. The presence of the magnetic field causes the percentage increase in average Nusselt number to be negative for other cases (M2, M3, and M4). Therefore, the presence of the magnetic field results in a reduction in the heat transfer rate in comparison with no magnetic field in these cases.

Table 7 The Effect of the Place of the Magnetic Field on the Heat Transfer and average temperature for $Mn_f^* = 10^4$, $d/L = 0.1$ and $Ha_f^* = 100$

	M1	M2	M3	M4
Nu_m	6.767	5.450	4.190	5.450
η	3	-21	-57	-21
θ_{avg}	0.238	0.228	0.148	0.228

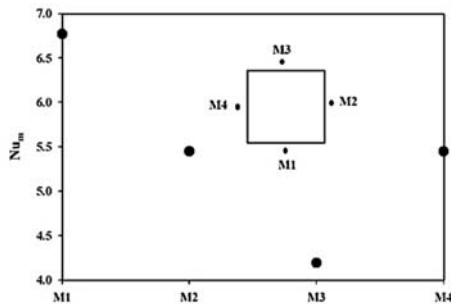
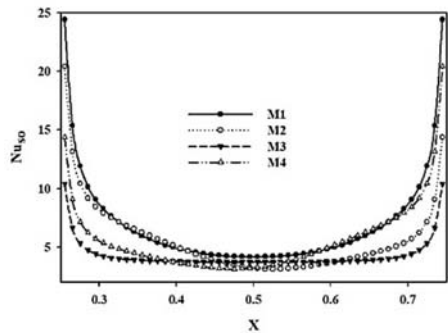


Fig. 4. The effect of the position of the magnetic field on the local Nusselt number on the heat source (top) and average Nusselt number (bottom) for $Mn_f^* = 10^4$, $d/L = 0.1$ and $Ha_f^* = 100$.

4.1.2. Displacement of the magnetic field source along the edges

In this section, the magnetic number of $Mn_f^* = 10^4$ and the vertical distance from the sides of the enclosure $d/L = 0.1$ are used to examine the effect of the position of the magnetic field along the sides AB, BC, CD and DA on the heat transfer for a constant Hartmann number of $Ha_f^* = 100$. Figure 6

shows the average Nusselt number for different positions of the magnetic field source along the sides of the enclosure.

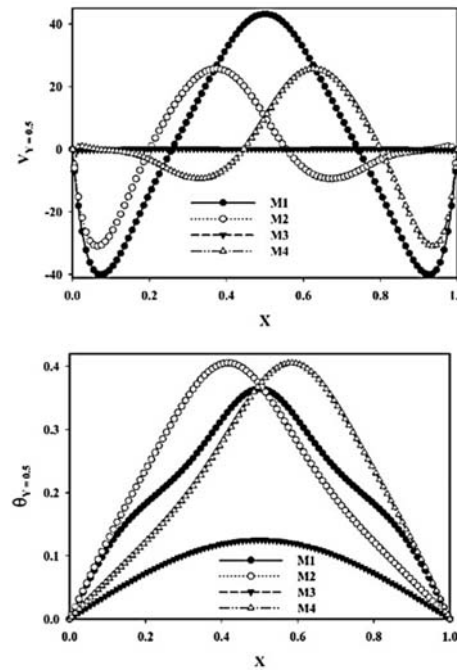


Fig. 5. The effect of the position of the magnetic field on vertical velocity at the central line of the enclosure $V_{y=0.5}$ (top) and temperature $\theta_{y=0.5}$ (bottom) for $Mn_f^* = 10^4$, $d/L = 0.1$ and $Ha_f^* = 100$.

The maximum heat transfer corresponds to the points A and B along the side AB. The heat transfer decreases by moving the magnetic field source to the center of the side AB. The displacement of the magnetic field location along the vertical sides of BC or DA leads to a maximum heat transfer at the bottom of the side (points A and B) due to the geometry symmetry. The displacement of the field along the side of the CD does not lead to a significant effect. In general, it can be concluded that the maximum heat transfer occurs in the bottom corners of the enclosure (points A and B).

4.1.3. Displacement of the magnetic field source along the normal direction to the edges

In this section, the magnetic field source is located at one of the four M1, M2, M3 and M4 points and the effect of the displacement of the magnetic field location along the normal direction to the sides of the enclosure (direction (d) in Fig. 1) is studied. The Hartmann number is $Ha_f^* = 100$ and the magnetic number is $Mn_f^* = 10^4$. Figure 7 shows the average Nusselt number versus the distance (d/L) from the center of the sides AB, BC, CD, and DA. As can be seen from this figure, at point M1 the maximum heat transfer is at a distance of 0.01. As the distance

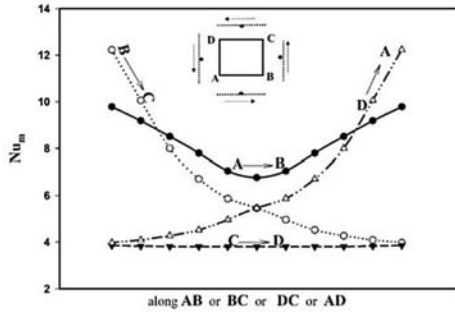


Fig. 6. Effect of the position of the magnetic field along the sides of the enclosure on the average Nusselt number for $Mn_f^* = 10^4$, $d/L = 0.1$ and $Ha_f^* = 100$.

increases, the heat transfer decreases due to the decrease in the strength of the magnetic field and therefore the magnetic field at a longer distance can not have a significant effect on the motion of the vortices. The heat transfer slightly increases at the points M2 or M4 by increasing the distance of the magnetic field from the BC or DA sides. It was noted that the presence of magnetic field at M2 or M4 points leads to a reduction in the heat transfer compared to no magnetic field at these points. Therefore, as the source distance from the sides increases, the higher heat transfer rate is expected. No significant change of heat transfer is observed at the point M3 by increasing d/L .

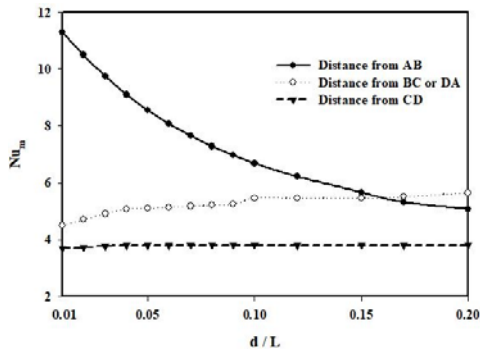


Fig. 7. Effect of the position of the magnetic field along the normal direction to the sides on the average Nusselt number for $Mn_f^* = 10^4$ and $Ha_f^* = 100$.

4.2. Effect of the magnetic and Hartmann numbers on the heat transfer and fluid flow

In this section, the effects of magnetic number variation due to FHD effects and the Hartmann number variation due to the MHD effects on heat transfer and fluid flow are discussed. In the previous sections, it was concluded that the maximum heat transfer in the enclosure was achieved by placing the magnetic field source in the corner of A, B. Also, the

optimal vertical distance of $d/L = 0.01$ was obtained for the maximum heat transfer from the sides of the enclosure. Considering the above-mentioned statements, the maximum temperature and Cartesian coordinates, and the symmetry of considered geometry, the heat transfer is studied by changing the magnetic number and Hartmann number at the point A near DA $(a, b) = (-0.01, 0)$, at the point A near AB $(a, b) = (0, -0.01)$ and the point M1 $(a, b) = (0.5, -0.01)$.

Table 8 shows the effects of magnetic number and Hartmann number on the heat transfer. There is no significant change in the heat transfer for different Mn_f^* and Ha_f^* at the corner points. However, the heat transfer initially decreases slightly, and then increases with the change of Mn_f^* at the point M1. Heat transfer also decreases by increasing Ha_f^* . Since the variations of Mn_f^* and Ha_f^* are significant at the point M1, the streamlines and isothermal lines are presented in Fig. 8 at this point.

Figure 8 shows the effect of Mn_f^* and Ha_f^* on the streamlines and isothermal lines. The vortices become stronger (increase in ψ_{max}) as Mn_f^* increases and the isothermal lines are dispersed more in the enclosure. These indicate an increase in the heat transfer. However, the vortices are weakened (decrease in ψ_{max}) by as Ha_f^* is increased and the isothermal lines are dispersed less in the enclosure. These indicate a decrease in the heat transfer. In general, the heat transfer in the enclosure, in addition to the buoyancy forces, is also due to the effect of FHD and MHD. The Kelvin force, which is due to the effects of the FHD, causes the flow of the inside of the enclosure to flow and the Lorentz force that is due to the MHD applied on the moving particles of the fluid. The vortices, which were initially formed in the enclosure due to the effects of buoyancy, are also affected by Kelvin and Lorentz forces. If these forces are exerted in the direction of the vortices, they will rotate more results in an increase in the heat transfer and vice versa.

5. CONCLUSIONS

Lubricants are mainly used in machine equipment to reduce friction and noise between surfaces. The use of free-flowing powders as main materials and additives in oils is a method to increase the thermal properties and stability of lubricants. Graphite slurry is one of the most widely used lubricants in the industry.

This paper presents a numerical study on the natural convective heat transfer of Fe_3O_4 /graphite slurry in a square cavity. The slurry was assumed to be a non-Newtonian ferrofluid and the cavity was considered under a magnetic field. The non-Newtonian parameters of the graphite slurry (a mixture of ethylene glycol and graphite powder) were determined using the experimental values. The computational governing equations were obtained and solved based on the effects of Ferrohydrodynamics (FHD), Magnetohydrodynamics (MHD) and non-Newtonian

Table 8 Effect of the magnetic number and the Hartmann number on the heat transfer for $d/L = 0.01, Ra_f^* = 10^5$.

	Num					
Mn_f^*	$Ha_f^* = 5$			$Ha_f^* = 100$		
	$(a, b) = (-0.01, 0)$	$(a, b) = (0, -0.01)$	$(a, b) = (0.5, -0.01)$	$(a, b) = (-0.01, 0)$	$(a, b) = (0, -0.01)$	$(a, b) = (0.5, -0.01)$
10^3	11.78	11.78	11.77	11.78	11.73	11.33
10^4	11.78	11.78	11.69	11.78	11.73	11.28
10^5	11.78	11.79	11.34	11.78	11.74	11.04
10^6	11.78	11.90	13.16	11.78	11.82	12.30

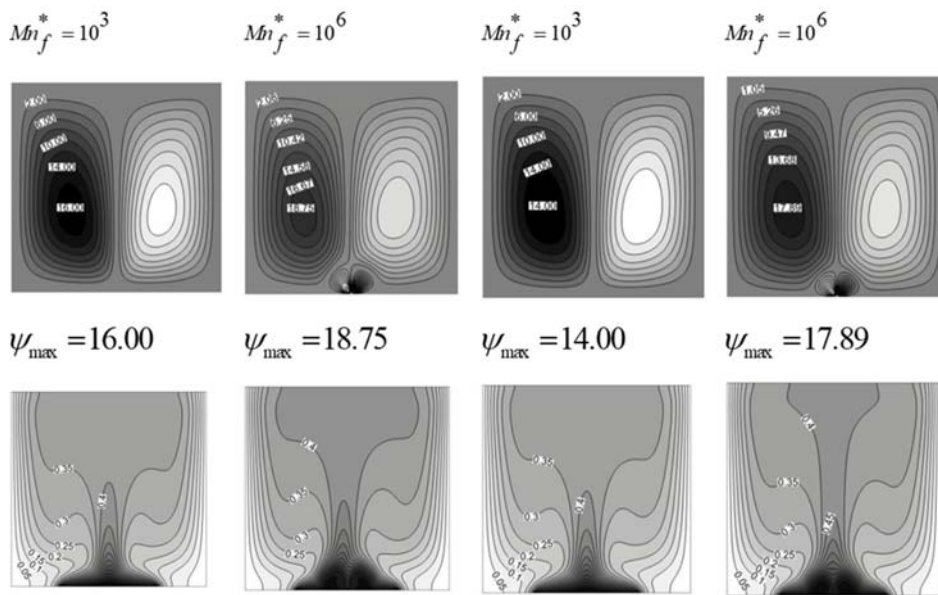


Fig. 8. Effect of the magnetic number and the Hartmann number on streamlines (top) and isothermal lines (bottom) at the point M1 and $d/L = 0.01$.

fluid behavior. The effects of magnetic field position and magnetic number due to the effects of FHD and Hartmann number due to MHD effects on heat transfer and fluid flow were investigated.

By placing the magnetic field source at the four sides of the enclosure at the points M1 to M4, it was concluded that the strength of the vortices and heat transfer rate increased in the case where the magnetic field source was located at the point M1, close to the heat source. The strength of the vortices and heat transfer rate decreased at three other points due to the distance from the source of heat generation.

Once the magnetic source was moved to the vicinity of the side AB, the maximum heat transfer rate was obtained for the location of magnetic source adjacent to the points A and B. In addition, due to the symmetry, the maximum heat transfer was observed at the points A and B along the sides BC or DA, and

no significant change was observed in the heat transfer by displacement of the magnetic field source along the side CD.

The maximum heat transfer was for the case $d/L = 0.01$. The heat transfer decreased with the increase of d/L from the side AB at the point M1 due to a decrease in the strength of the magnetic field by increasing the distance. The magnetic field did not have a significant effect on the vortex movement. At the points M2 or M4 point, the heat transfer slightly increased with increasing the distance of the magnetic field source from the sides BC or DA. At the point M3, there was no considerable change in heat transfer.

The heat transfer in the enclosure, in addition to the buoyancy forces, depended on the effect of FHD and MHD. The Kelvin force, due to the FHD effects, caused the flow of the inside of the enclosure to flow

and the Lorentz force, due to the MHD applied on the moving particles of the fluid. The vortices, which were initially formed in the enclosure due to the effects of buoyancy, were also affected by Kelvin and Lorentz forces. If these forces are exerted in the direction of the vortices, they will rotate more results in an increase in the heat transfer and vice versa.

By changing Mn_f^* and Ha_f^* , when the magnetic field source was located at the bottom corner of the enclosure, there was no significant change in the heat transfer. However, when the magnetic field source was placed at the point M1, the heat transfers initially reduced slightly and then increased. Under these conditions, heat transfer decreased with Ha_f^*

REFERENCES

- Aminossadati, S. M., B. Ghasemi and A. Kargar (2014). Computational Analysis of Magneto-hydrodynamic Natural Convection in a Square Cavity with a Thin Fin. *European Journal of Mechanics, B/Fluids* 46, 154–63.
- Aminossadati, S. M., A. Raisi and B. Ghasemi (2011). Effects of Magnetic Field on Nanofluid Forced Convection in a Partially Heated Microchannel. *International Journal of Non-Linear Mechanics* 46(10), 1373–82.
- Anon (2015). "POCO Graphit." *An Entegris Company* 1–39. Retrieved (<http://poco.com/tabid/65/Default.aspx>).
- Anon (n.d.) *Ethylene Glycol Heat-Transfer Fluid - Engineering ToolBox*, https://www.Meglobal.Biz/Media/Product...MEGGlobal_MEG.Pdf.
- Asfer, M., M. Balkrishna, A. Kumar, S. Khandekar and P. K. Panigrahi (2016). Effect of Magnetic Field on Laminar Convective Heat Transfer Characteristics of Ferrofluid Flowing through a Circular Stainless Steel Tube. *International Journal of Heat and Fluid Flow* 59, 74–86.
- Ashouri, M., B. Ebrahimi, M. B. Shafii, M. H. Saidi and M. S. Saidi (2010). Correlation for Nusselt Number in Pure Magnetic Convection Ferrofluid Flow in a Square Cavity by a Numerical Investigation. *Journal of Magnetism and Magnetic Materials* 322(22), 3607–13.
- Bandyopadhyay, T. K. and S. K. Das (2013). Non-Newtonian and Gas-Non-Newtonian Liquid Flow through Elbows - CFD Analysis. *Journal of Applied Fluid Mechanics* 6(1), 131–41.
- Blaney, L. (2007). Magnetite (Fe₃O₄): Properties, Synthesis, and Applications. *Lehigh University Lehigh Preserve* 15, 33–81.
- Bourada, A., A. Boutra, K. Bouarnouna, D. E. Ameziani and Y. K. Benkahla (2020). Natural Convection of Power Law Fluid through a Porous Deposit: MRT-LBM Approach. *Journal of Applied Fluid Mechanics* 14(2), 459–72.
- Brandão, P. V. and Mohamed. O. (2021). Darcy–Carreau Model and Nonlinear Natural Convection for Pseudoplastic and Dilatant Fluids in Porous Media. *Transport in Porous Media* 136(2), 521–39.
- Dareing, D. W. and R. D. Dayton (1992). Non-Newtonian Behavior of Powder Lubricants Mixed with Ethylene Glycol. *Tribology Transactions* 35(1), 114–20.
- Ghalambaz, M., S. A. M. Mehryan, R. Kalantar Feroz, A. Hajjar, I. Hashim and R. Babaei Mahani (2020). Free Convective Heat Transfer of a Non-Newtonian Fluid in a Cavity Containing a Thin Flexible Heater Plate: An Eulerian–Lagrangian Approach. *Journal of Thermal Analysis and Calorimetry* (0123456789).
- Ghasemi, B. (2005). Mixed Convection in a Rectangular Cavity with a Pulsating Heated Electronic Component. *Numerical Heat Transfer, Part A* 47(5), 505–21.
- Ghasemi, B., S. M. Aminossadati and A. Raisi (2011). Magnetic Field Effect on Natural Convection in a Nanofluid-Filled Square Enclosure. *International Journal of Thermal Sciences* 50(9), 1748–1756.
- Guha, A. and K. Pradhan (2014). Natural Convection of Non-Newtonian Power-Law Fluids on a Horizontal Plate. *International Journal of Heat and Mass Transfer* 70, 930–38.
- Kasaiepoor, A., B. Ghasemi and S. M. Aminossadati. (2015). Convection of Cu-Water Nanofluid in a Vented T-Shaped Cavity in the Presence of Magnetic Field. *International Journal of Thermal Sciences* 94, 50–60.
- Kefayati, G. H. R. (2014). Simulation of Non-Newtonian Molten Polymer on Natural Convection in a Sinusoidal Heated Cavity Using FDLBM. *Journal of Molecular Liquids* 195, 165–74.
- Kumari, S. and P. V. S. N. Murthy (2018). Stability of Vertical Throughflow of a Power Law Fluid in Double Diffusive Convection in a Porous Channel. *Journal of Applied Fluid Mechanics* 11(2), 497–505.
- Lemus-Mondaca, R. A., N. O. Moraga and J. Riquelme (2013). Unsteady 2D Conjugate Natural Non-Newtonian Convection with Non-Newtonian Liquid Sterilization in Square Cavity. *International Journal of Heat and Mass Transfer* 61, 73–81.
- Mahmoudi, A. H., I. Pop, M. Shahi and F. Talebi (2013). MHD Natural Convection and Entropy Generation in a Trapezoidal Enclosure Using Cu-Water Nanofluid. *Computers and Fluids* 72, 46–62.
- Matin, M. Habibi, I. Pop and S. Khanchezar (2013). Natural Convection of Power-Law Fluid between Two-Square Eccentric Duct Annuli. *Journal of Non-Newtonian Fluid Mechanics* 197, 11–23.
- Moraga, N. O., G. P. Parada and D. A. Vasco (2016).

- Power Law Non-Newtonian Fluid Unsteady Conjugate Three-Dimensional Natural Convection inside a Vessel Driven by Surrounding Air Thermal Convection in a Cavity. *International Journal of Thermal Sciences* 107, 247–58.
- Mostofizadeh, A., Y. Li, B. Song and Y. Huang (2011). Synthesis, Properties, and Applications of Low-Dimensional Carbon-Related Nanomaterials. *Journal of Nanomaterials* 201(1), 1-21.
- Patankar, S. (1980). *Numerical Heat Transfer and Fluid Flow*. New York: CRC press.
- Pishkar, I., B. Ghasemi, A. Raisi and S. M. Aminossadati (2019). Numerical Study of Unsteady Natural Convection Heat Transfer of Newtonian and Non-Newtonian Fluids in a Square Enclosure under Oscillating Heat Flux. *Journal of Thermal Analysis and Calorimetry* 138(2), 1697–1710.
- Rahman, M. M., H. F. Öztöp, R. Saidur, S. Mekhilef and K. Al-Salem (2013). Finite Element Solution of MHD Mixed Convection in a Channel with a Fully or Partially Heated Cavity. *Computers & Fluids* 79, 53–64.
- Raisi, A., S. M. Aminossadati and B. Ghasemi (2016). An Innovative Nanofluid-Based Cooling Using Separated Natural and Forced Convection in Low Reynolds Flows. *Journal of the Taiwan Institute of Chemical Engineers* 62, 259–66.
- Rashad, A. M. (2017). Impact of Thermal Radiation on MHD Slip Flow of a Ferrofluid over a Non-Isothermal Wedge. *Journal of Magnetism and Magnetic Materials* 422, 25–31.
- Rosensweig, R. E. (2013). *Ferrohydrodynamics*. Courier Corporation.
- Selimefendigil, F. and H. F. Öztöp (2014). Forced Convection of Ferrofluids in a Vented Cavity with a Rotating Cylinder. *International Journal of Thermal Sciences* 86, 258–75.
- Selimefendigil, F., H. F. Öztöp and K. Al-Salem (2014). Natural Convection of Ferrofluids in Partially Heated Square Enclosures. *Journal of Magnetism and Magnetic Materials* 372, 122–33.
- Sheisheikholeslami, M. and D. Domiri Ganji (2014). Ferrohydrodynamic and Magnetohydrodynamic Effects on Ferrofluid Flow and Convective Heat Transfer. *Energy* 75, 400–410.
- Turan, O., A. Sachdeva, N. Chakraborty and R. J. Poole (2011). Laminar Natural Convection of Power-Law Fluids in a Square Enclosure with Differentially Heated Side Walls Subjected to Constant Temperatures. *Journal of Non-Newtonian Fluid Mechanics* 166(17), 1049–63.
- Tzirtzilakis, E. E. (2005). A Mathematical Model for Blood Flow in Magnetic Field. *Physics of Fluids* 17(7), 77103.
- Tzirtzilakis, E. E. and M. A. Xenos (2013). Biomagnetic Fluid Flow in a Driven Cavity. *Meccanica* 48(1), 187–200.
- Vinogradov, I., L. Khezzar and D. Siginer (2011). Heat Transfer of Non-Newtonian Dilatant Power Law Fluids in Square and Rectangular Cavities. *Journal of Applied Fluid Mechanics* 4(2-s 1), 37–42.
- Westrum Jr, E. F. and F. Grønvold (1969). Magnetite (Fe₃O₄) Heat Capacity and Thermodynamic Properties from 5 to 350 K, Low-Temperature Transition. *The Journal of Chemical Thermodynamics* 1(6), 543–57.
- Yarahmadi, M., H. Moazami Goudarzi and M. B. Shafii. (2015). Experimental Investigation into Laminar Forced Convective Heat Transfer of Ferrofluids under Constant and Oscillating Magnetic Field with Different Magnetic Field Arrangements and Oscillation Modes. *Experimental Thermal and Fluid Science* 68, 601–11.
- Yue, H., Y. Zhao, X. Ma and J. Gong (2012). Ethylene Glycol: Properties, Synthesis, and Applications. *Chemical Society Reviews* 41(11), 4218–44.
- Zhang, H., T. Xu, X. Zhang, L. Zheng, Y. Wang and Y. Zong (2015). Numerical Study on the Skin Friction and Heat Transfer Coefficient of Non-Newtonian Power Law Fluid in Boundary Layer. *Procedia Engineering* 121, 824–29.